Quantum correlation between longitudinal-mode intensities in a multimode squeezed semiconductor laser

Shuichiro Inoue and Hitoshi Ohzu
Department of Applied Physics, Waseda University, Shinjuku, Tokyo 169, Japan

Susumu Machida and Yoshihisa Yamamoto
NTT Basic Research Laboratories, Musashino-Shi, Tokyo 180, Japan
(Received 21 January 1992)

The intensity-noise properties of a constant-current-driven multimode semiconductor laser were studied theoretically and experimentally. It was shown that the total intensity noise of a pump-noise-suppressed multimode semiconductor laser was reduced to below the standard quantum limit even though the intensity noise of each individual mode had large excess intensity noise. This discovery stems from negative quantum correlations between longitudinal-mode intensities.

PACS number(s): 42.50.Dv, 42.55.Px

I. INTRODUCTION

It has been predicted theoretically that the intensity fluctuation on the field emitted from a pump-noise-suppressed single-mode laser operating at well above the threshold is reduced to below the standard quantum limit (SQL) [1]. In the case of a semiconductor injection laser, the pump noise is easily suppressed to below the shot-noise level by a high-impedance constant-current source [2]. Light from such a constant-current-driven semiconductor laser featuring squeezed intensity fluctuations has been experimentally demonstrated [3–6]. More recently, intensity noise that was reduced to below the SQL by more than 10 dB has been demonstrated [7]. In these experiments, the spectrum of the semiconductor laser usually featured a single longitudinal mode.

However, we have recently observed that the intensity squeezing is observed not only in a single-mode-oscillation case but also in a multimode-oscillation case. This intensity squeezing in a multimode oscillation is due to the negative quantum correlations between the intensity fluctuations of different longitudinal modes. In a two-mode optical parametric oscillator, it has been demonstrated that the signal and the idler intensity fluctuations exhibit the positive quantum correlations and the noise on the intensity difference between the two beams is reduced below the shot-noise value [8].

In this paper we will show that a pump-noise-suppressed multimode semiconductor laser produces the negative quantum correlations between the intensity fluctuations of different longitudinal modes. Because of this quantum correlation, the total intensity noise is suppressed to below the shot-noise value, even though the intensity noise of each longitudinal mode is much higher than the shot-noise value.

II. LANGEVIN EQUATIONS FOR A MULTIMODE SEMICONDUCTOR LASER

In order to analyze the quantum-noise properties of a multimode semiconductor laser, we employ the operator Langevin equations. There are four assumptions for our analytical model.

(1) The total number of the lasing modes is three, that is, one main mode and two side modes.

(2) The stimulated emission gain of the main mode is slightly higher than those of the side modes due to a finite-gain bandwidth. The stimulated-emission gains of the two side modes are the same. The difference between the main-mode gain and the side-mode gain results in the difference between the spontaneous-emission coefficients of those modes because of Einstein's relationship for A and B coefficients.

(3) All modes have the same output coupling (mirror) loss and internal loss.

(4) Ideal population inversion is created in the active layer, so the stimulated absorption rate is neglected.

All of these assumptions are a fairly good approximation for the experimental results using a GaAs transverse-junction-stripe laser operated at 60 K, which will be presented later. We derive the multimode Langevin equations for the internal photon number of each mode and the total excited electron number. The relation between the internal and external fields and the correlation functions for the noise sources are used to calculate the external intensity spectral densities of each longitudinal mode and the correlation spectral densities between different longitudinal modes.

A. Multimode Langevin equations and correlation functions for the noise operators

The multimode Langevin equations for the cavity internal photon-number operator $\hat{n}_i$, is given by

$$\frac{d\hat{n}_i}{dt}=\left[\tilde{A}_i(N_c)-\frac{1}{\tau_p}\right]\hat{n}_i+\tilde{E}_{cv,i}+\tilde{G}_i(t)+\hat{g}_i(t)+\hat{f}_i(t)\ . \tag{2.1}$$

Here the subscript i indicates the ith longitudinal mode. $1/\tau_p$ is the photon decay rate, which is decomposed into the internal loss contribution $1/\tau_{po}$ and the output cou-

pling contribution $1/\tau_{pe}$ as

$$\frac{1}{\tau_p}=\frac{1}{\tau_{po}}+\frac{1}{\tau_{pe}} . \tag{2.2}$$

$\tilde{A}_i(N_c)$ is the stimulated emission rate per lasing photon, which is equal to the spontaneous emission rate $\tilde{E}_{cv,i}$ due to Einstein's relationship,

$$\tilde{A}_i(N_c)=\tilde{E}_{cv,i} . \tag{2.3}$$

Here we assume the ideal population inversion and so neglect the stimulated absorption rate $\tilde{E}_{vc,i}$. The noise operators $\tilde{G}_i(t)$, $\hat{g}_i(t)$, and $\hat{f}_i(t)$ are associated with the random processes of stimulated-emission gain, internal loss, and output coupling (mirror) loss. The correlation functions for these noise operators are

$$\langle \tilde{G}_i(t)\tilde{G}_i(u)\rangle=\delta(t-u)\langle \tilde{E}_{cv,i}\rangle\langle \hat{n}_i\rangle , \tag{2.4}$$

$$\langle \hat{g}_i(t)\hat{g}_i(u)\rangle=\delta(t-u)\frac{1}{\tau_{po}}\langle \hat{n}_i\rangle , \tag{2.5}$$

$$\langle \hat{f}_i(t)\hat{f}_i(u)\rangle=\delta(t-u)\frac{1}{\tau_{pe}}\langle \hat{n}_i\rangle . \tag{2.6}$$

The noise operator $\hat{f}_i$ represents the contribution of the zero-point fluctuation $\hat{f}_e$ coupled into the cavity through the partially reflecting mirror. We use a tilde to denote the operators for the electron system and a caret to denote the operators for the field system. The Langevin equation for the total excited electron-number operator $\tilde{N}_c(t)$ is given by

$$\frac{d\tilde{N}_c(t)}{dt}=P-\frac{\tilde{N}_c}{\tau_{\rm sp}}-\tilde{A}_1(N_c)\hat{n}_1-\tilde{A}_2(N_c)\hat{n}_2-\tilde{A}_3(N_c)\hat{n}_3-\tilde{E}_{cv}+\tilde{\Gamma}_p(t)+\tilde{\Gamma}_{\rm sp}(t)+\tilde{\Gamma}(t) , \tag{2.7}$$

where P is the pumping rate and $\tau_{\rm sp}$ is the spontaneous-emission lifetime of the electrons. $\tilde{E}_{cv}$ is the spontaneous-emission rate into all the lasing modes,

$$\tilde{E}_{cv}=\tilde{E}_{cv,1}+\tilde{E}_{cv,2}+\tilde{E}_{cv,3} , \tag{2.8}$$

while $\tilde{N}_c/\tau_{\rm sp}$ is the spontaneous-emission rate into all nonlasing modes. $\tilde{\Gamma}_p(t)$, $\tilde{\Gamma}_{\rm sp}(t)$, and $\tilde{\Gamma}(t)$ are fluctuating-noise operators. $\tilde{\Gamma}_p(t)$ is the pump noise, $\tilde{\Gamma}_{\rm sp}(t)$ is the spontaneous-emission noise, and $\tilde{\Gamma}(t)$ is the stimulated-emission noise. The correlation functions for these noise operators are

$$\langle \tilde{\Gamma}_p(t)\tilde{\Gamma}_p(u)\rangle=\begin{cases}0, & \text{pump-noise-suppressed laser}\\ \delta(t-u)P, & \text{shot-noise-limited pump laser}\end{cases} , \tag{2.9}$$

$$\langle \tilde{\Gamma}_{\rm sp}(t)\tilde{\Gamma}_{\rm sp}(u)\rangle=\delta(t-u)\frac{\langle \tilde{N}_c\rangle}{\tau_{\rm sp}} , \tag{2.10}$$

$$\langle \tilde{\Gamma}(t)\tilde{\Gamma}(u)\rangle=\delta(t-u)(\langle \tilde{E}_{cv,1}\rangle\langle \hat{n}_1\rangle+\langle \tilde{E}_{cv,2}\rangle\langle \hat{n}_2\rangle+\langle \tilde{E}_{cv,3}\rangle\langle \hat{n}_3\rangle) . \tag{2.11}$$

Since the two operators $\tilde{G}_i(t)$ and $\tilde{\Gamma}(t)$ come from the same origin (the stimulated-emission processes), they have the correlation

$$\langle \tilde{G}_i(t)\tilde{\Gamma}(u)\rangle=-\delta(t-u)\langle \tilde{E}_{cv,i}\rangle\langle \hat{n}_i\rangle . \tag{2.12}$$

B. Noise spectral densities

Let us consider a laser oscillator pumped at well above the threshold. For this region, the operator Langevin equations (2.1) and (2.7) can be solved by the quasilinearization procedure. We expand the operators into c-number mean values and fluctuating operators according to

$$\tilde{N}_c(t)=N_{c0}+\Delta\tilde{N}_c(t) , \tag{2.13}$$

$$\hat{n}_i(t)=n_{i0}+\Delta\hat{n}_i=a_{i0}^2+2a_{i0}\Delta\hat{a}_i(t) , \tag{2.14}$$

$$\tilde{A}_i(N_c)=\langle \tilde{A}_i\rangle+\frac{d\langle \tilde{A}_i\rangle}{dN_{c0}}\Delta\tilde{N}_c . \tag{2.15}$$

Here N_{c0}, a_{i0}, and n_{i0} are the average excited electron number, field intensity, and photon number. $\Delta\tilde{N}_c$, $\Delta\hat{a}_i$, and $\Delta\hat{n}_i$ are the Hermitian excited-electron-number, field-intensity and photon-number operators. Substituting (2.13), (2.14), and (2.15) into (2.1) and (2.7), and neglecting the terms in the order of Δ^2, we obtain the following linearized operator equations:

$$\frac{d\Delta\hat{a}_i}{dt}=A_1\Delta\hat{a}_i+A_2\Delta\tilde{N}_c+\frac{1}{2a_{i0}}[\tilde{G}_i(t)+\hat{g}_i(t)+\hat{f}_i(t)] , \tag{2.16}$$

$$\frac{d\Delta\tilde{N}_c}{dt}=A_3\Delta\tilde{N}_c+A_4\Delta\hat{a}_1+A_5\Delta\hat{a}_2+A_5\Delta\hat{a}_3+\tilde{\Gamma}_p(t)+\tilde{\Gamma}_{\rm sp}(t)+\tilde{\Gamma}(t) , \tag{2.17}$$

where

$$A_1=\frac{\beta_i N_{c0}}{\tau_{\rm sp}}-\frac{1}{\tau_p} , \tag{2.18}$$

$$A_2=\frac{a_{i0}\beta_i}{2\tau_{\rm sp}} , \tag{2.19}$$

$$A_3=-\left[\frac{1}{\tau_{\rm sp}}+\frac{\beta n_{10}}{\tau_{\rm sp}}+\frac{m\beta(n_{20}+n_{30})}{\tau_{\rm sp}}\right] , \tag{2.20}$$

$$A_4=-2a_{10}\frac{\beta N_{c0}}{\tau_{\rm sp}} , \tag{2.21}$$

$$A_5=-2a_{20}\frac{m\beta N_{c0}}{\tau_{sp}} . \tag{2.22}$$

Here β_i is the spontaneous-emission coefficient of the ith mode. We also used the following relation:

$$\langle \tilde{A}_i \rangle=\langle \tilde{E}_{cv,i} \rangle=\frac{\beta_i N_{c0}}{\tau_{sp}} , \tag{2.23}$$

$$\beta_1=\beta \text{ (main mode)} , \tag{2.24}$$

$$\beta_2=\beta_3=m\beta \text{ (side mode)} , \tag{2.25}$$

where $m<1$. Fourier transforms of (2.16) and (2.17) are expressed as

$$i\Omega\Delta\hat{a}_i(\Omega)=A_1\Delta\hat{a}_i(\Omega)+A_2\Delta\tilde{N}_c(\Omega)+\frac{1}{2a_{i0}}[\tilde{G}_i(\Omega)+\hat{g}_i(\Omega)+\hat{f}_i(\Omega)] \tag{2.26}$$

and

$$i\Omega\Delta\tilde{N}_c(\Omega)=A_3\Delta\tilde{N}_c(\Omega)+A_4\Delta\hat{a}_1(\Omega)+A_5\Delta\hat{a}_2(\Omega)+A_5\Delta\hat{a}_3(\Omega)+\tilde{\Gamma}_p(\Omega)+\tilde{\Gamma}_{sp}(\Omega)+\tilde{\Gamma}(\Omega) . \tag{2.27}$$

To simplify the analysis we solve these equations in the limit of $\Omega\rightarrow 0$. From these equations $\tilde{N}_c(0)$ is eliminated, and the expression for the internal intensity noise $\Delta\hat{a}_i(0)$ is obtained as

$$\Delta\hat{a}_i(0)=C_i[\alpha_1\hat{H}_{r1}(0)+\alpha_2\hat{H}_{r2}(0)+\alpha_2\hat{H}_{r3}(0)+\alpha_3\tilde{F}(0)]+D_i\hat{H}_{ri}(0) , \tag{2.28}$$

where

$$\hat{H}_{ri}(0)=\frac{1}{2a_{i0}}[\tilde{G}_i(0)+\hat{g}_i(0)+\hat{f}_i(0)] , \tag{2.29}$$

$$\tilde{F}(0)=\tilde{\Gamma}_p(0)+\tilde{\Gamma}_{sp}(0)+\tilde{\Gamma}(0) . \tag{2.30}$$

TABLE I. Expressions for the coefficients C_i, D_i, α_i, E_i, and F_i defined in the text.

Symbol	Expression
C_1	$\frac{a_{10}\beta\tau_p}{2(\tau_{sp}-\beta N_{c0}\tau_p)}$
C_2	$\frac{a_{20}m\beta\tau_p}{2(\tau_{sp}-m\beta N_{c0}\tau_p)}$
D_1	$\frac{\tau_{sp}\tau_p}{\tau_{sp}-\beta N_{c0}\tau_p}$
D_2	$\frac{\tau_{sp}\tau_p}{\tau_{sp}-m\beta N_{c0}\tau_p}$
α_1	$-\frac{2a_{10}D_1\beta N_{c0}}{1+\beta n_{10}+2\beta N_{c0}a_{10}C_1+2m\beta(n_{20}+2N_{c0}a_{20}C_2)}$
α_2	$-\frac{2ma_{20}D_2\beta N_{c0}}{1+\beta n_{10}+2\beta N_{c0}a_{10}C_1+2m\beta(n_{20}+2N_{c0}a_{20}C_2)}$
α_3	$\frac{\tau_s}{1+\beta n_{10}+2\beta N_{c0}a_{10}C_1+2m\beta(n_{20}+2N_{c0}a_{20}C_2)}$
E_1	$(a_{10}C_1+a_{20}C_2+a_{30}C_3)\alpha_1+a_{10}D_1$
E_2	$(a_{10}C_1+a_{20}C_2+a_{30}C_3)\alpha_2+a_{20}D_2$
E_3	$(a_{10}C_1+a_{20}C_2+a_{30}C_3)\alpha_3$
F_1	$2C_2\alpha_1$
F_2	$2C_2\alpha_2+D_2$
F_3	$2C_2\alpha_3$

The expressions for the coefficients C_i, D_i, and α_i are given in the Table I.

The output field-intensity fluctuation is expressed in terms of the internal field fluctuation and the incident (and reflected) zero-point fluctuation as

$$\Delta\hat{r}_i(t)=\left[\frac{1}{\tau_{pe}}\right]^{1/2}\Delta\hat{a}_i(t)-\frac{\hat{f}_i(t)}{(1/\tau_{pe})^{1/2}} . \tag{2.31}$$

Substituting (2.28) into the Fourier transform of (2.31), we obtain

$$\Delta\hat{r}_i(0)=-\frac{\hat{f}_i(0)}{(1/\tau_{pe})^{1/2}}+\left[\frac{1}{\tau_{pe}}\right]^{1/2}\{C_i[\alpha_1\hat{H}_{r1}(0)+\alpha_2\hat{H}_{r2}(0)+\alpha_2\hat{H}_{r3}(0)+\alpha_3\tilde{F}(0)]+D_i\hat{H}_{ri}(0)\} . \tag{2.32}$$

The resulting expressions for the intensity-noise spectral densities of each longitudinal mode and the total modes are given by

$$P_{\Delta\hat{r}_1}(0)=\frac{1}{2}\left[\frac{\tau_{pe}-C_1\alpha_1-D_1}{\tau_{pe}}\right]^2+\left[\frac{\alpha_2C_1}{\tau_{pe}}\right]^2+\frac{(C_1\alpha_1+D_1)^2+2\alpha_2^2C_1^2}{2\tau_{pe}\tau_{po}}+\frac{2\beta N_{c0}}{\tau_{sp}\tau_{pe}}\left[\frac{\alpha_1C_1+D_1}{2}-\alpha_3a_{10}C_1\right]^2+\frac{4m\beta N_{c0}}{\tau_{sp}\tau_{pe}}\left[\frac{C_1\alpha_2}{2}-\alpha_3a_{20}C_1\right]^2+\frac{2\alpha_3^2C_1^2}{\tau_{pe}}\left[P+\frac{N_{c0}}{\tau_{sp}}\right] , \tag{2.33}$$

$$P_{\Delta\hat{r}_2}(0)=\frac{1}{2}\left[\frac{\tau_{pe}-C_2\alpha_2-D_2}{\tau_{pe}}\right]^2+\frac{1}{2\tau_{pe}\tau_{po}}(C_2\alpha_2+D_2)^2+\frac{C_2^2}{2\tau_{pe}}(\alpha_1^2+\alpha_2^2)\left[\frac{1}{\tau_{po}}+\frac{1}{\tau_{pe}}\right]+\frac{2m\beta N_{c0}}{\tau_{sp}\tau_{pe}}\left[\frac{C_2\alpha_2+D_2}{2}-C_2\alpha_3a_{20}\right]^2+\frac{2\beta N_{c0}}{\tau_{sp}\tau_{pe}}\left[\frac{C_2\alpha_1}{2}-C_2\alpha_3a_{10}\right]^2+\frac{2m\beta N_{c0}}{\tau_{sp}\tau_{pe}}\left[\frac{C_2\alpha_2}{2}-C_2\alpha_3a_{20}\right]^2+\frac{2C_2^2\alpha_3^2}{\tau_{pe}}\left[P+\frac{N_{c0}}{\tau_{sp}}\right] , \tag{2.34}$$

and

$$P_{\Delta\hat{r}}(0)=\frac{2}{n_{10}+2n_{20}}\left[\left[\frac{\tau_{pe}a_{10}-E_1}{2\tau_{pe}}\right]^2+2\left[\frac{\tau_{pe}a_{20}-E_2}{2\tau_{pe}}\right]^2+\frac{\beta N_{c0}}{\tau_{sp}\tau_{pe}}\left[\frac{E_1}{2}-E_3a_{10}\right]^2\right.$$
$$\left.+\frac{2m\beta N_{c0}}{\tau_{sp}\tau_{pe}}\left[\frac{E_2}{2}-E_3a_{20}\right]^2+\frac{E_1^2+2E_2^2}{4\tau_{pe}\tau_{po}}+\frac{E_3^2}{\tau_{pe}}\left[P+\frac{N_{c0}}{\tau_{sp}}\right]\right], \tag{2.35}$$

where

$$\Delta\hat{r}=\Delta\hat{r}_1+\Delta\hat{r}_2+\Delta\hat{r}_3\ . \tag{2.36}$$

The expressions for the coefficients E_i are given in Table I.

C. Cross-correlation spectral densities

In order to study the correlation between different longitudinal-mode intensity fluctuations, we calculate the cross correlations. The resulting expression for the cross correlations are

$$\langle\Delta\hat{r}_1(0)\Delta\hat{r}_2(0)\rangle=\frac{1}{\tau_{pe}}\left[\frac{1}{\tau_{pe}}+\frac{1}{\tau_{po}}\right][C_1C_2(\alpha_1^2+2\alpha_2^2)+C_2\alpha_1D_1+C_1\alpha_2D_2]-\frac{C_1\alpha_2+C_2\alpha_1}{\tau_{pe}}$$
$$+\frac{C_2\beta N_{c0}}{\tau_{sp}\tau_{pe}}[\alpha_1(C_1\alpha_1+D_1-4C_1\alpha_3a_{10})-2\alpha_3(D_1a_{10}-2C_1\alpha_3n_{10})]$$
$$+\frac{C_1m\beta N_{c0}}{\tau_{sp}\tau_{pe}}[\alpha_2(C_2\alpha_2+D_2-4C_2\alpha_3a_{20})-2\alpha_3(D_2a_{20}-2C_2\alpha_3n_{20})]$$
$$+\frac{4C_1C_2}{\tau_{pe}}\left[\left[\frac{\alpha_2^2}{4}+\alpha_3^2n_{20}-\alpha_2\alpha_3a_{20}\right]\frac{m\beta N_{c0}}{\tau_{sp}}+\alpha_3^2\left[P+\frac{N_{c0}}{\tau_{sp}}\right]\right], \tag{2.37}$$

$$\langle\Delta\hat{r}_1(0)\Delta\hat{r}_{23}(0)\rangle=\frac{F_1(C_1\alpha_1+D_1)}{\tau_{pe}}\left[\frac{1}{\tau_{pe}}+\frac{1}{\tau_{po}}+\frac{\beta N_{c0}}{\tau_{sp}}\right]+\frac{2F_2C_1\alpha_2}{\tau_{pe}}\left[\frac{1}{\tau_{pe}}+\frac{1}{\tau_{po}}+\frac{m\beta N_{c0}}{\tau_{sp}}\right]$$
$$+\frac{4F_3C_1\alpha_3}{\tau_{pe}}\left[\frac{\beta N_{c0}n_{10}}{4\tau_{sp}}+\frac{m\beta N_{c0}n_{20}}{\tau_{sp}}+P+\frac{N_{c0}}{\tau_{sp}}\right]$$
$$-\frac{F_1+2C_1\alpha_2}{\tau_{pe}}-\frac{2a_{10}\beta N_{c0}}{\tau_{sp}\tau_{pe}}[F_3(C_1\alpha_1+D_1)+F_1\alpha_3C_1]-\frac{4m\beta N_{c0}a_{20}}{\tau_{sp}\tau_{pe}}(F_3C_1\alpha_2+F_2C_1\alpha_3)\ , \tag{2.38}$$

where

$$\Delta\hat{r}_{23}(0)=\Delta\hat{r}_2(0)+\Delta\hat{r}_3(0)\ . \tag{2.39}$$

The expressions for the coefficients F_i are given in Table I.

III. NUMERICAL RESULTS

A. Steady-state lasing characteristics

When we obtain the linearized operator equations (2.16) and (2.17), we also obtain the following steady-state equations:

$$0=P-\frac{N_{c0}}{\tau_{sp}}-(\langle\tilde{A}_1\rangle n_{10}+\langle\tilde{A}_2\rangle n_{20}+\langle\tilde{A}_3\rangle n_{30})-\langle E_{cv}\rangle\ , \tag{3.1}$$

$$0=\left[\langle\tilde{A}_i\rangle-\frac{1}{\tau_p}\right]n_{i0}+\langle\tilde{E}_{cv,i}\rangle\ . \tag{3.2}$$

We solve the steady-state equations (3.1) and (3.2) numerically. The following numerical parameters are assumed: $\tau_{sp}=1\times10^{-9}$ s, $\tau_{pe}=1\times10^{-12}$ s, $\tau_{po}\gg\tau_{pe}$, $\beta=1\times10^{-4}$, $m=0.999\,95$ (case 1), and $m=0.995$ (case 2). In case 1, we assume the stimulated-emission gain for the main mode is higher than that for the side mode only by a factor of 10^{-5}. This assumption is based on the model for the Gaussian gain-envelope function with 300-Å gain width and the longitudinal-mode separation of 3 Å. In case 2, the difference of the stimulated-emission gain between the main mode and the side mode is larger than that in case 1 by a factor 10^2. Figure 1 shows the steady-state photon numbers and the total excited-electron number as function of a pumping rate (electrons/sec). At the threshold (10^{16} electrons/sec), the three modes have roughly equal photon number. At well above the threshold, the photon number of the main mode is much higher than that of the side mode. It is shown that the three-mode laser oscillation is well modeled by introducing the different β values for the main and side modes. The ratio

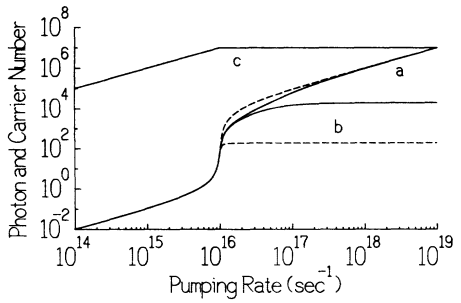

FIG. 1. The steady-state photon numbers of the main mode (a) and the side mode (b) and the total excited-electron number (c) as a function of a pumping rate (electron/sec). Numerical parameters are as follows: $\tau_{sp}=1\times10^{-9}$ s, $\tau_{pe}=1\times10^{-12}$ s, $\tau_{po}\gg\tau_{pe}$, $\beta=1\times10^{-4}$, $m=0.999\,95$ (solid line), and $m=0.995$ (dashed line).

between the photon numbers n_{10} of the main mode and n_{20} of the side mode at a certain pumping rate is determined by the ratio m between β_1 and β_2.

B. The external intensity-noise spectral densities

The external intensity-noise spectral densities are given by (2.33), (2.34), and (2.35). We calculate these noise spectral densities numerically under the assumption that the pumping noise is suppressed completely. The numerical parameters are the same as those of the previous subsection. Figure 2 shows the external intensity-noise spectral densities as a function of a pumping level. In case 2, the intensity-noise spectral densities are much smaller than those in case 1. This is due to the larger gain difference between the main mode and the side mode. It is demonstrated that the external intensity-noise spectral density of each individual mode is much larger than the standard quantum limit (SQL), but the total external intensity-noise spectral density is reduced to below the SQL as the pumping level increases. This result suggests that the intensity squeezing will be observed for a pump-noise-suppressed multimode semiconductor laser only when the total intensity is measured.

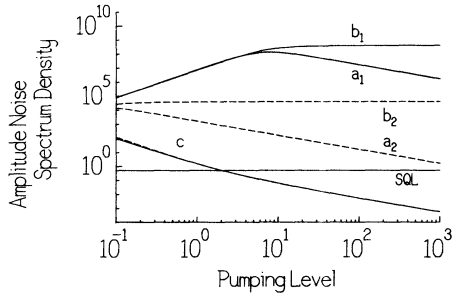

FIG. 2. The external intensity-noise spectral densities at $\Omega\simeq0$ of the main mode (a_1) and (a_2), the side mode (b_1) and (b_2), and the total modes (c) as a function of a normalized pumping level $I/I_{th}-1$. The solid line corresponds to $m=0.9995$ and the dashed line to $m=0.995$.

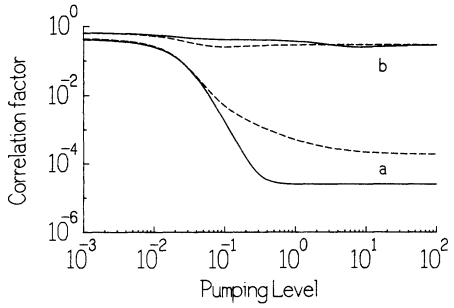

FIG. 3. The cross-correlation spectral densities at $\Omega\simeq0$ as a function of a normalized pumping level $I/I_{th}-1$. The ordinate is spectral density plus one, the cross correlation $P_{\Delta r_1\Delta r_2}(\Omega)/[P_{\Delta r_1}(\Omega)P_{\Delta r_2}(\Omega)]^{1/2}+1$ is plotted. The solid line corresponds to $m=0.999\,95$ and the dashed line to $m=0.995$. a: The cross-correlation spectral density between the main mode and the sum of the two side modes. b: The cross-correlation spectral density between the main mode and one side mode.

C. Cross-correlation spectral densities

The cross correlation between the main mode and one side mode is given by (2.37), and the cross correlation between the main mode and the sum of the two side modes is given by (2.38). We calculate these cross-correlation spectral densities numerically under the assumption that the pumping noise is completely suppressed. The numerical parameters are the same as those of the previous analysis. Figure 3 shows the cross-correlation spectral densities as a function of a pumping level. Here we normalize the cross correlation by $[P_{\Delta\hat{r}_1}(0)P_{\Delta\hat{r}_2}(0)]^{1/2}$ and $[P_{\Delta\hat{r}_1}(0)P_{\Delta\hat{r}_{23}}(0)]^{1/2}$, respectively. This figure demonstrates that the negative correlation is formed between the main mode and the side mode at above the threshold. The very strong negative correlations on the order of -0.9999 (case 1) and -0.999 (case 2) is formed between the main mode and the sum of the two sidemodes. This difference of the order of negative correlation between

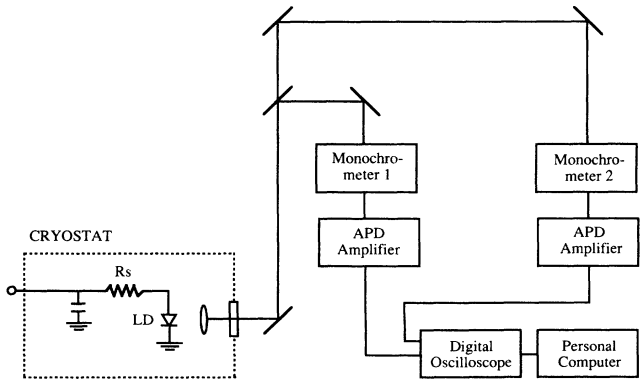

FIG. 4. The experimental setup for the measurement of the cross correlation between the intensity fluctuations of the two longitudinal modes (LD denotes laser diode, APD denotes avalanche photodiode).

case 1 and case 2 corresponds to that of the intensity-noise spectral densities. The physical origin for such negative correlation is the cross-gain saturation; that is, the increase (or decrease) of the spontaneous-emission coupling to the main mode makes the intensity of the main mode higher (or lower); then the gain of the side mode is suppressed (or enhanced). This noise-reduction mechanism is true of the more general case in which the number of the lasing mode is more than three and their gain profiles are asymmetric, as far as the gain is homogeneously broadened. This is the reason why the total intensity-noise spectral density is suppressed to below the SQL as the pumping level increases, even though the intensity-noise spectral densities of the individual modes are much larger than the SQL.

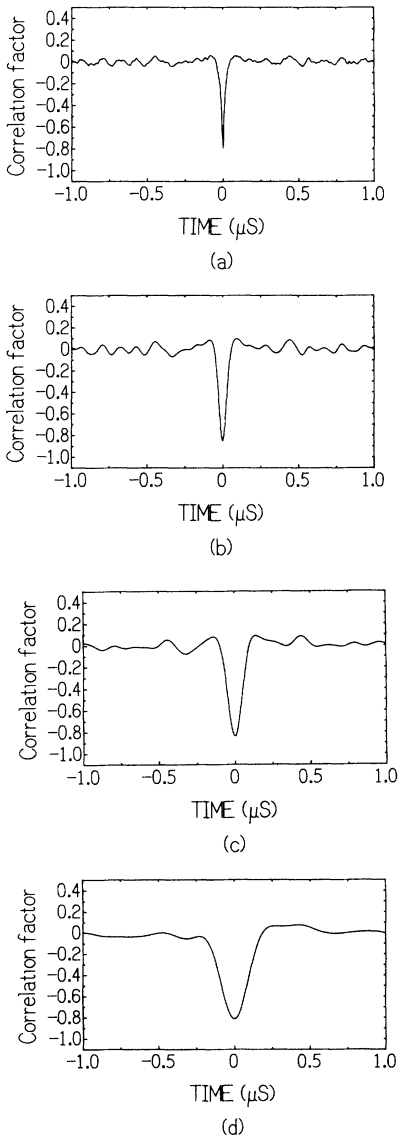

FIG. 5. The measured cross correlation factors $C_{v_1v_2}(\tau)$ for various low-pass-filter bandwidths B. (a) $B=70$ MHz, (b) $B=10$ MHz, (c) $B=4$ MHz, and (d) $B=2$ MHz.

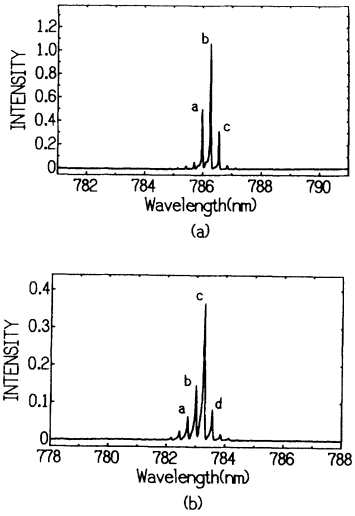

FIG. 6. The spectra of the semiconductor laser in the two different injection currents I and temperatures T. (a) $I=6.5$ mA, $T=60$ K and (b) $I=10$ mA, $T=20$ K.

IV. EXPERIMENT

We performed two experiments for a pump-noise-suppressed multimode semiconductor laser. One is the measurement of the total intensity-noise level normalized by the SQL. This experiment was performed by the same procedure as the previous experiment [7]. The other is the measurement of the cross correlation between the two longitudinal-mode intensity fluctuations.

A. Experimental setup and data analyzing procedure

The experimental setup for the measurement of the cross correlation is shown in Fig. 4. The semiconductor

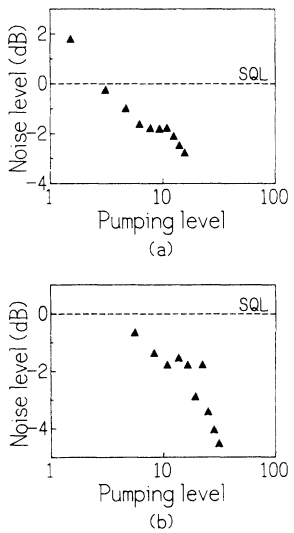

FIG. 7. The measured total intensity-noise level normalized by the shot-noise level as a function of the normalized pumping level $I/I_{th}-1$. (a) $T=60$ K, $I_{th}=0.7$ mA, and (b) $T=20$ K, $I_{th}=0.4$ mA.

laser, the high-impedance bias circuit, and the collimating microlens are mounted inside a cryostat. A GaAs transverse-junction-stripe semiconductor laser (Mitsubishi model ML-3308) was used at 20–70 K. Two modes are selected by monochrometer 1 and 2 and then detected by the Si avalanche photodiodes (APD's). The intensity fluctuations of these modes are amplified and memorized in a dual-channel digital oscilloscope. The sampling time of the digital oscilloscope is 5 nsec. The data memorized in the digital oscilloscope are analyzed by a personal computer.

Cross-correlation function is defined by

$$C_{v_1 v_2}(\tau)=\int_{-\infty}^{\infty} v_1(t)v_2^*(t-\tau)dt \ , \tag{4.1}$$

where $v_1(t)$ and $v_2(t)$ are the intensity fluctuations. In order to obtain this cross-correlation function, we use the following relation:

$$\hat{C}_{v_1 v_2}(\tau)=\hat{v}_1(\omega)\hat{v}_2^*(\omega) \ , \tag{4.2}$$

where the caret denotes the Fourier transform of the function. The data analyzing procedure is follows. The measured intensity fluctuations $v_1(t)$ and $v_2(t)$ memorized in the digital oscilloscope are Fourier transformed and low-pass filtered by a computer. Then, we calculate the right-hand side of (4.2), and the product is inversely Fourier transformed. The low-pass filtering is performed to exclude the high-frequency noncorrelated fluctuation components and to view only low-frequency correlated components. Figure 5 shows the cross correlation between the two intensity fluctuations for the different filter bandwidths. This figure demonstrates that the correlation time depends on the filter bandwidth, that is, the correlation time becomes longer as the filter bandwidth becomes narrower.

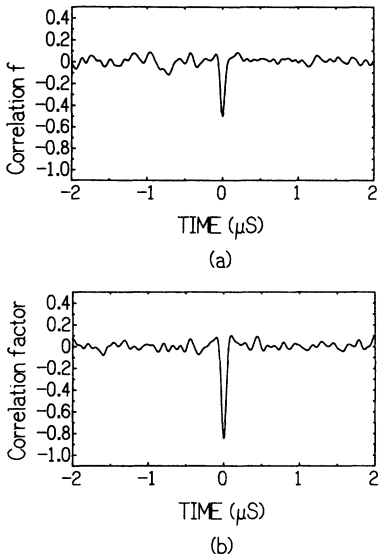

FIG. 9. The cross correlation between the main-mode and the side-mode intensity fluctuations at $I=6.5$ mA and $T=60$ K. The bandwidth of the low-pass filter is $B=10$ MHz. Complete negative correlation is expressed by -1. (a) The cross correlation between the mode b and the mode c and (b) the cross correlation between the mode b and the mode a.

B. Experimental results

Experimental results are classified into two cases. One is the case that the intensity-noise spectral density of the main mode is the largest. The other is that the intensity-noise spectral density of the side mode is larger than that of the main mode. The experimental results of these two cases indicate how the negative correlations are formed and the total intensity noise is squeezed.

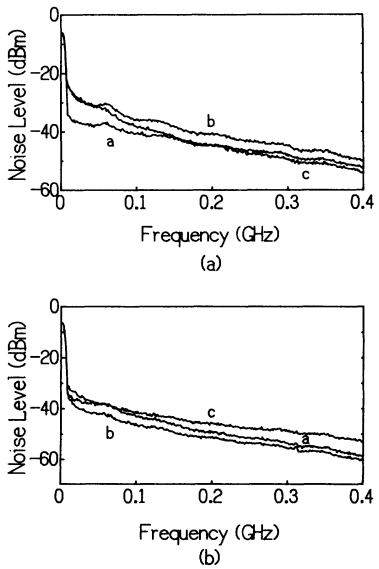

FIG. 8. The measured intensity-noise spectral densities of the three individual longitudinal modes at $I=6.5$ mA and $T=60$ K. (a) Measured noise spectra and (b) noise spectra normalized by the corresponding photocurrents.

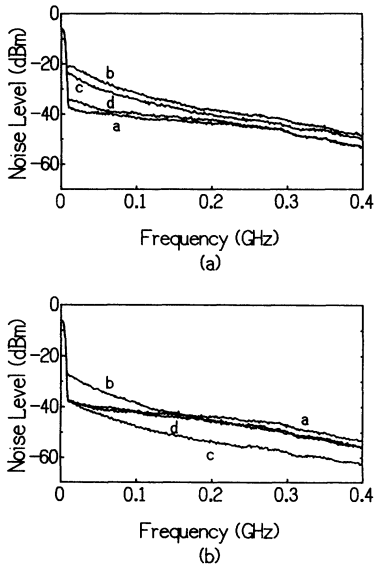

FIG. 10. The intensity-noise spectral densities of the four individual longitudinal modes at 10 mA and $T=20$ K. (a) The measured noise spectra and (b) the noise spectra normalized by the corresponding photocurrents.

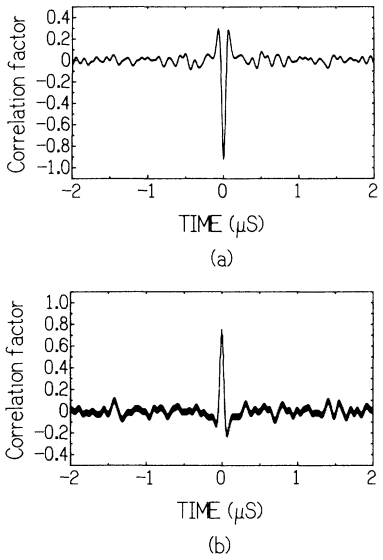

FIG. 11. The cross correlation between the intensity fluctuations of the two longitudinal modes at $I=10$ mA and $T=20$ K. The bandwidth of the low-pass filter is $B=10$ MHz. (a) The cross correlation between mode b and mode c and (b) the cross correlation between mode c and mode d.

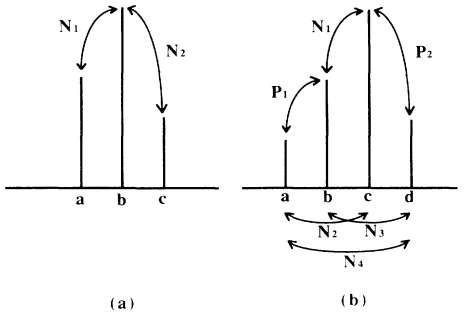

FIG. 12. Summary of the cross correlation measurements for two cases. N_i and P_i denote the negative and positive correlations. (a) $I=6.5$ mA, $T=60$ K, $N_1=-0.85$ and $N_2=-0.50$. (b) $I=10$ mA, $T=20$ K, $N_1=-0.93$, $N_2=-0.82$, $N_3=-0.76$, $N_4=-0.76$, $P_1=0.72$, and $P_2=0.57$.

First we show the experimental results of the former case. Figure 6(a) shows the spectrum of the laser oscillation modes driven by a dc current of 6.5 mA at 60 K. This spectrum corresponds to our analytical model presented in the previous section. Figure 7(a) shows the total intensity-noise level normalized by the SQL as a function of the pumping level. Figures 6(a) and 7(a) demonstrate that the intensity squeezing was observed for the pump-noise-suppressed multimode semiconductor laser if we measure the total intensity noise. Figure 8(a) shows the intensity-noise spectral densities of the three longitudinal modes. The normalized intensity-noise spectral densities by the corresponding photocurrents are shown in Fig. 8(b). These noise characteristics also correspond to the theoretical model of the previous section (Fig. 2). Figures 9(a) and 9(b) show the cross correlation between the main mode and the two side-mode intensity fluctuations. These figures demonstrate that there are negative correlations between the intensity fluctuations of the main mode and the side mode. This experimental result is in agreement with the numerical results (Fig. 3).

Next we show the experimental results for the latter case. Figure 6(b) shows the spectrum of the laser oscillation modes driven by a higher dc current of 10 mA at a lower temperature of 20 K. Figure 7(b) shows the total intensity-noise level normalized by the SQL as a function of the pumping level. The intensity squeezing was also observed. Figures 10(a) and 10(b) show the intensity-noise spectral densities and the normalized ones by the photocurrents. Figure 10(a) shows that the intensity-noise spectral density of the main mode [10(c)] is smaller than that of the side mode [10(b)]. Figures 11(a) and 11(b) show the cross correlation between the intensity fluctuations of the two longitudinal modes. The negative correlations are not always formed between the intensity fluctuations of the main mode and the side mode. There exists also the positive correlation for such a complicated spectrum case. Figure 12 summarizes the two experimental results. Figure 12(b) shows that there are positive correlations between mode a and mode b and also between mode c and mode d. On the other hand, there are the negative correlations between all the other combinations. This means that the intensity fluctuations of one group (modes b and a) are compensated for by the other group (modes c and d). By means of these negative correlations between the two groups, the total intensity fluctuations are reduced to below the SQL.

V. CONCLUSION

The intensity squeezing was observed not only for a single longitudinal-mode semiconductor laser but also for a multimode semiconductor laser. However, the intensity fluctuation of each longitudinal mode is much larger than the SQL. This paper demonstrates theoretically and experimentally that the total intensity fluctuation is reduced to below the SQL because of the quantum-mechanical negative correlations between the longitudinal modes. These quantum mechanical negative correlations are to be formed between the noisiest mode and the other modes.

The semiconductor laser used in this experiment has a highly doped active layer ($P\simeq 10^{19}$ cm^{-3}), so the gain profile is expected to be nearly homogeneously broadened even at a low temperature. This is the reason why there exists the correlation between the intensity fluctuations of the different longitudinal modes. If the gain medium is inhomogeneously broadened, the correlation will disappear. In this case, the total intensity fluctuation will not be reduced. This was also confirmed in a multimode semiconductor laser with a nondoped active layer.

[1] Y. Yamamoto, S. Machida, and O. Nilsson, Phys. Rev. A **34**, 4025 (1986).
[2] Y. Yamamoto and S. Machida, Phys. Rev. A **35**, 5114 (1987).
[3] S. Machida, Y. Yamamoto, and Y. Itaya, Phys. Rev. Lett. **58**, 1000 (1987).
[4] S. Machida and Y. Yamamoto, Phys. Rev. Lett. **60**, 792 (1988).
[5] S. Machida and Y. Yamamoto, Opt. Lett. **14**, 1045 (1989).
[6] W. H. Richardson, and R. M. Shelby, Phys. Rev. Lett. **64**, 400 (1990).
[7] W. H. Richardson, S. Machida, and Y. Yamamoto, Phys. Rev. Lett. **66**, 2867 (1991).
[8] A. Heidmann *et al.*, Phys. Rev. Lett. **59**, 2555 (1987).